DALTON

Asymmetric functionalisation of aza macrocycles. Syntheses, crystal structures and electrochemistry of $[Ni(Bz[9]aneN_3)_2][PF_6]_2$ and $[Pd(Bz[9]aneN_3)_2][PF_6]_2 \cdot 2MeCN$ ($Bz[9]aneN_3$ = 1-benzyl-1,4,7-triazacyclononane) †

Alexander J. Blake, Ian A. Fallis, Simon Parsons, Steven A. Ross and Martin Schröder *

Department of Chemistry, The University of Edinburgh, West Mains Road, Edinburgh EH9 3JJ, UK

1-Benzyl-1,4,7-triazacyclononane ($Bz[9]aneN_3$) has been prepared and its co-ordination chemistry with Ni^{II} and Pd^{II} investigated. The crystal structure of the complex $[Ni(Bz[9]aneN_3)_2][PF_6]_2$ revealed six independent Ni–N distances, affording a distorted-octahedral co-ordination geometry. Four lie in the range 2.089(4)–2.123(4) Å, while the distances to the benzyl amine N-donors are significantly longer at 2.262(4) and 2.251(4) Å. The benzyl amine N-donors occupy adjacent sites at the metal centre affording a *syn* geometry. Cyclic voltammetry of $[Ni(Bz[9]aneN_3)_2][PF_6]_2$ in MeCN at a platinum electrode showed a reversible Ni^{II}–Ni^{III} oxidation at $E_{\frac{1}{2}} = +0.76$ V *vs.* ferrocene–ferrocenium at 235 K. This process was irreversible at higher temperatures. The ESR spectrum of $[Ni(Bz[9]aneN_3)_2]^{3+}$ exhibits an axial signal, with $g_{\|} = 2.03$ and $g_{\perp} = 2.15$, consistent with a tetragonally elongated octahedral co-ordination geometry at Ni^{III}. The crystal structure of $[Pd(Bz[9]aneN_3)_2][PF_6]_2 \cdot 2MeCN$ revealed the Pd atom on an inversion centre with the ligands bound *via* two N-donors from each, Pd–N 2.0588(19) and 2.0605(19) Å. The benzyl amine N-donors do not interact with the metal centre, Pd · · · N 3.402(4) Å. Cyclic voltammetry of $[Pd(Bz[9]aneN_3)_2][PF_6]_2$ in MeCN showed a reversible Pd^{II}–Pd^{III} couple at $E_{\frac{1}{2}} = +0.36$ V at 298 K. The ESR spectrum of $[Pd(Bz[9]aneN_3)_2]^{3+}$ exhibits an axial signal, with $g_{\|} = 2.007$ and $g_{\perp} = 2.117$. Superhyperfine coupling ($A_{\|} = 26.9$ G) is observed to two N-donors in the axial component consistent with a tetragonally elongated octahedral co-ordination geometry at the Pd^{III}.

The co-ordination chemistry of the facially binding triaza-macrocycle 1,4,7-triazacyclononane ($[9]aneN_3$) has been comprehensively established over the last twenty years.[1-3] Sandwich complexes of general formula $[M([9]aneN_3)_2]^{x+}$ are thus well known to represent kinetically inert, thermodynamically stable systems. More recently, *N*-functionalisation of $[9]aneN_3$ *via* incorporation of 'innocent' alkyl substituents such as methyl,[4] isopropyl[5] and benzyl[6] groups has been reported. One important feature of the co-ordination chemistry of these *N*-functionalised compounds is their inability to form sandwich complexes, which has been attributed to steric interactions between the bulky substituents.[1] Macrocycles such as $Me_3[9]aneN_3$ (1,4,7-trimethyl-1,4,7-triazacyclononane) therefore serve as analogues for face-capping ligands such as tris(pyrazolyl)borate[7] and cyclopentadiene,[8,9] allowing variation of the donor array at one face of a metal whilst protecting the other face.

We were interested in the co-ordination properties of mono *N*-functionalised derivatives of $[9]aneN_3$ in order to ascertain whether the preparation of sandwich complexes of the type $[M(Bz[9]aneN_3)_2]^{x+}$ would be possible, and to observe the degree of steric strain which might be induced in such species. We report herein the synthesis of 1-benzyl-1,4,7-triazacyclononane ($Bz[9]aneN_3$) and its complexation with Ni^{II} and Pd^{II}. These two ions were chosen because their co-ordination chemistry with $[9]aneN_3$ is well established and also because they show strong stereochemical requirements for different co-ordination geometries, namely octahedral and square planar respectively.

Results and Discussion

Scheme 1 illustrates the preparation of $Bz[9]aneN_3$, *via* reaction of 1,4,7-triazatricyclo[5.2.1.$0^{4,10}$]decane[10-13] with $PhCH_2Br$, to afford the previously reported compound

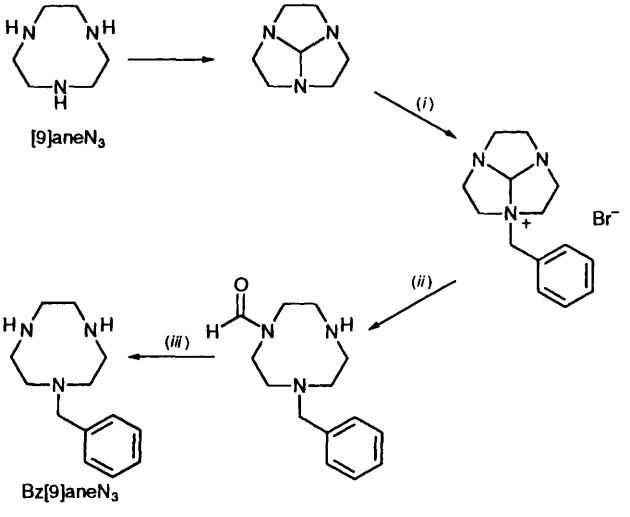

Scheme 1 The preparation of $Bz[9]aneN_3$ from $[9]aneN_3$. (*i*) $PhCH_2Br$, tetrahydrofuran (thf), 1 h; (*ii*) water, reflux, 3.5 h; (*iii*) KOH, EtOH, reflux, 24 h

1-benzyl-4-formyl-1,4,7-triazacyclononane.[14,15] The ^1H and ^{13}C NMR spectra of the latter are complicated by the presence of two isomeric forms in solution, due to the slow rotation about the C–N amide bond. Base hydrolysis of this intermediate with KOH–EtOH yields $Bz[9]aneN_3$ in high yield.

Nickel

The reaction of Ni^{II} with $Bz[9]aneN_3$ was undertaken in order to compare its complexation behaviour with that of $[9]aneN_3$.

† *Non-SI unit employed:* G = 10^{-4} T.

Table 1 Selected bond lengths (Å) and angles (°) for $[Ni(Bz[9]aneN_3)_2]^{2+}$

Ni–N(23)	2.089(4)	N(1)–C(2)	1.490(6)	N(7)–C(8)	1.491(6)	C(19)–N(20)	1.476(6)
Ni–N(7)	2.091(4)	N(1)–C(10)	1.498(6)	C(8)–C(9)	1.497(7)	N(20)–C(21)	1.490(6)
Ni–N(20)	2.101(4)	C(2)–C(3)	1.517(7)	C(10)–C(11)	1.504(7)	C(21)–C(22)	1.508(7)
Ni–N(4)	2.123(4)	C(3)–N(4)	1.476(6)	N(17)–C(25)	1.473(6)	C(22)–N(23)	1.481(6)
Ni–N(17)	2.251(4)	N(4)–C(5)	1.499(6)	N(17)–C(18)	1.496(6)	N(23)–C(24)	1.482(6)
Ni–N(1)	2.262(4)	C(5)–C(6)	1.514(7)	N(17)–C(26)	1.503(6)	C(24)–C(25)	1.531(6)
N(1)–C(9)	1.490(6)	C(6)–N(7)	1.487(6)	C(18)–C(19)	1.489(7)	C(26)–C(27)	1.505(7)
N(23)–Ni–N(7)	178.8(2)	N(17)–Ni–N(1)	108.95(14)	N(7)–C(6)–C(5)	110.1(4)	C(19)–C(18)–N(17)	111.1(4)
N(23)–Ni–N(20)	81.8(2)	C(9)–N(1)–C(2)	111.2(4)	C(6)–N(7)–C(8)	112.7(4)	N(20)–C(19)–C(18)	110.5(4)
N(7)–Ni–N(20)	99.2(2)	C(9)–N(1)–C(10)	110.7(4)	C(6)–N(7)–Ni	105.8(3)	C(19)–N(20)–C(21)	112.7(4)
N(23)–Ni–N(4)	99.2(2)	C(2)–N(1)–C(10)	110.2(4)	C(8)–N(7)–Ni	112.4(3)	C(19)–N(20)–Ni	107.1(3)
N(7)–Ni–N(4)	81.3(2)	C(9)–N(1)–Ni	102.4(3)	N(7)–C(8)–C(9)	113.5(4)	C(21)–N(20)–Ni	110.9(3)
N(20)–Ni–N(4)	90.2(2)	C(2)–N(1)–Ni	106.8(3)	N(1)–C(9)–C(8)	112.7(4)	N(20)–C(21)–C(22)	111.2(4)
N(23)–Ni–N(17)	80.87(14)	C(10)–N(1)–Ni	115.2(3)	N(1)–C(10)–C(11)	118.6(4)	N(23)–C(22)–C(21)	110.7(4)
N(7)–Ni–N(17)	98.8(2)	N(1)–C(2)–C(3)	113.0(4)	C(25)–N(17)–C(18)	110.6(4)	C(22)–N(23)–C(24)	112.5(4)
N(20)–Ni–N(17)	80.3(2)	N(4)–C(3)–C(2)	109.8(4)	C(25)–N(17)–C(26)	111.5(4)	C(22)–N(23)–Ni	105.0(3)
N(4)–Ni–N(17)	170.3(2)	C(3)–N(4)–C(5)	113.9(4)	C(18)–N(17)–C(26)	109.8(4)	C(24)–N(23)–Ni	113.3(3)
N(23)–Ni–N(1)	97.7(2)	C(3)–N(4)–Ni	106.5(3)	C(25)–N(17)–Ni	102.5(3)	N(23)–C(24)–C(25)	111.6(4)
N(7)–Ni–N(1)	81.3(2)	C(5)–N(4)–Ni	111.0(3)	C(18)–N(17)–Ni	107.6(3)	N(17)–C(25)–C(24)	111.7(4)
N(20)–Ni–N(1)	170.6(2)	N(4)–C(5)–C(6)	110.7(4)	C(26)–N(17)–Ni	114.7(3)	N(17)–C(26)–C(27)	116.8(4)
N(4)–Ni–N(1)	80.7(2)						

Table 2 Atomic coordinates (× 10^4) for $[Ni(Bz[9]aneN_3)_2]^{2+}$

Atom	*x*	*y*	*z*	Atom	*x*	*y*	*z*
Ni	985(1)	1 290(1)	8 273(1)	C(24)	517(4)	3 352(4)	7 581(3)
N(1)	2 302(3)	907(3)	7 984(2)	C(25)	1 352(3)	3 462(3)	8 385(3)
C(2)	2 044(4)	1(4)	7 470(3)	C(26)	2 172(3)	2 725(4)	9 702(3)
C(3)	954(4)	−157(4)	7 073(3)	C(27)	2 479(3)	3 710(4)	10 122(3)
N(4)	496(3)	−80(3)	7 662(2)	C(28)	3 158(4)	4 301(4)	9 970(3)
C(5)	719(4)	−943(4)	8 227(3)	C(29)	3 466(5)	5 198(5)	10 361(4)
C(6)	1 007(4)	−574(4)	9 068(3)	C(30)	3 105(6)	5 513(5)	10 898(4)
N(7)	1 670(3)	301(3)	9 204(2)	C(31)	2 438(5)	4 943(6)	11 072(4)
C(8)	2 666(4)	17(4)	9 259(3)	C(32)	2 137(4)	4 023(5)	10 689(3)
C(9)	3 051(3)	670(4)	8 776(3)	P(1)	5 404(1)	2 230(1)	260(1)
C(10)	2 649(3)	1 726(4)	7 594(3)	F(1)	5 276(2)	1 172(2)	−147(2)
C(11)	3 451(3)	1 497(4)	7 302(3)	F(2)	5 545(3)	3 296(2)	691(2)
C(12)	4 420(4)	1 418(4)	7 802(3)	F(3)	4 507(2)	2 024(3)	508(2)
C(13)	5 130(4)	1 226(6)	7 508(4)	F(4)	6 115(2)	1 759(2)	1 081(2)
C(14)	4 889(5)	1 138(5)	6 701(5)	F(5)	4 688(3)	2 727(3)	−540(2)
C(15)	3 957(5)	1 234(5)	6 205(4)	F(6)	6 308(2)	2 444(3)	29(2)
C(16)	3 231(4)	1 410(4)	6 500(3)	P(2)	2 164(1)	626(1)	1 550(1)
N(17)	1 272(3)	2 731(3)	8 961(2)	F(7)	1 483(2)	463(3)	2 042(2)
C(18)	400(3)	2 948(4)	9 160(3)	F(8)	2 810(3)	793(3)	1 044(2)
C(19)	−154(4)	2 016(4)	9 153(3)	F(9)	1 240(2)	487(4)	764(2)
N(20)	−351(3)	1 457(3)	8 412(2)	F(10)	3 086(3)	733(3)	2 331(2)
C(21)	−1 078(3)	1 965(4)	7 713(3)	F(11)	2 343(3)	−534(3)	1 571(3)
C(22)	−720(3)	2 035(4)	7 044(3)	F(12)	1 994(4)	1 777(3)	1 537(3)
N(23)	329(3)	2 288(3)	7 344(2)				

The structure and properties of $[Ni([9]aneN_3)_2]^{2+}$ have been reported previously by several workers,[16–21] with the single-crystal structure showing[17] an average Ni–N bond length of 2.10 Å. Hancock has suggested[22] that the ideal M–N bond length in complexes of the type $[M([9]aneN_3)_2]^{n+}$ is of the order 2.08 Å. Shorter lengths result in unfavourable steric interactions between the macrocyclic rings, whilst longer ones reduce the strength of the metal–ligand interaction. Thus, the Ni–N bond length in $[Ni([9]aneN_3)_2]^{2+}$ appears to be very close to optimal.

Reaction of $[Ni(H_2O)_6][NO_3]_2$ with 2 molar equivalents of $Bz[9]aneN_3$ in EtOH affords a pink precipitate which was dissolved in water. Addition of NH_4PF_6 gave a precipitate which was recrystallised from water–acetone to afford pink needles. The FAB mass spectrum of this material shows peaks which were assigned to $[Ni(Bz[9]aneN_3)_2]^+$ and $[Ni(Bz[9]aneN_3)_2(PF_6)]^+$ and analytical data confirmed the assignment of the product as $[Ni(Bz[9]aneN_3)_2][PF_6]_2$.

The electronic absorption spectrum of $[Ni(Bz[9]aneN_3)_2][PF_6]_2$ in MeCN exhibits three absorption maxima at ν_{max} 10 408 (ε = 11), 11 904 (sh), 18 798 (6) and 25 641 cm^{-1} (18 $dm^3\ mol^{-1}\ cm^{-1}$) consistent with octahedral co-ordination geometry at Ni^{II}. The shoulder on the low-energy ($^3A_{2g} \longrightarrow {}^3T_{2g}$) band is attributed to the spin-forbidden $^3A_{2g} \longrightarrow {}^1E_{2g}$ transition.[23,24] The absorption spectrum of $[Ni(Bz[9]aneN_3)_2]^{2+}$ contrasts with that reported by Yang and Zompa[16] for $[Ni([9]aneN_3)_2]^{2+}$ which exhibits maxima at ν_{max} 11 500 (sh), 12 500 (ε = 9), 20 000 (9) and 32 300 cm^{-1} (12 $dm^3\ mol^{-1}\ cm^{-1}$). The value for $10Dq$ of 10 408 cm^{-1} for $[Ni(Bz[9]aneN_3)_2]^{2+}$ (taken from the lowest-energy transition) is significantly lower than the value of 12 500 cm^{-1} reported for $[Ni([9]aneN_3)_2]^{2+}$.[25] This suggests that the steric bulk of $Bz[9]aneN_3$ (in comparison to $[9]aneN_3$) prevents the N-donors of the ligand approaching the optimum Ni–N distance of 2.08 Å.[22] This would result in a weaker ligand field and thus a smaller value of $10Dq$.

Assuming that $Bz[9]aneN_3$ is co-ordinated to the Ni^{II} in a facial manner (since the absorption data indicate that the species is octahedral), then two stereoisomers of the complex $[Ni(Bz[9]aneN_3)_2]^{2+}$ are possible. These are the *syn* and *anti* isomers illustrated in Fig. 1. The *syn* isomer has the benzyl amine donors occupying adjacent sites at the metal centre,

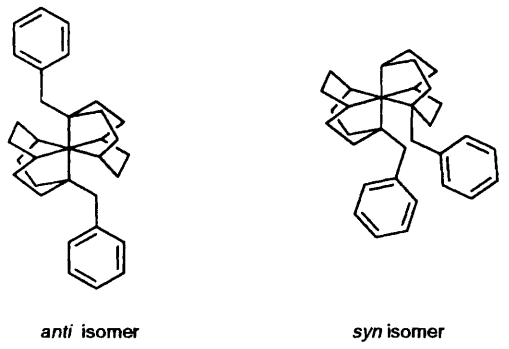

Fig. 1 Possible *syn* and *anti* isomers of $[Ni(Bz[9]aneN_3)_2]^{2+}$

whereas the *anti* isomer has the benzyl amines occupying opposite sites at the metal centre. One might initially expect the *anti* configuration to be the more favoured product on steric grounds as the bulky benzyl groups would be directed away from each other. In order to confirm the stereochemistry at the metal centre, a single-crystal structure determination was undertaken.

Pink needles of diffraction quality were obtained by evaporation of a water–MeCN solution of the complex. Details of the structure solution and refinement are given in the Experimental section. Selected bond lengths and angles are presented in Table 1, fractional atomic coordinates in Table 2 and a view of the cation in Fig. 2. The molecule possesses no crystallographically imposed symmetry, thus every atom is unique. The benzyl amines of the macrocycle are bound to the Ni^{II} at adjacent co-ordination sites, affording the *syn* isomer of the complex. There are two sets of Ni–N bond lengths. Four [N(4), N(7), N(20) and N(23)] lie in the range 2.089(4)–2.123(4) Å, whilst the two to the benzyl amines [N(1) and N(17)] are significantly longer at 2.262(4) and 2.251(4) Å respectively. The longer bond lengths are attributed in part to the steric bulk of the benzyl groups, which prevent the benzyl N atoms from approaching the metal centre. This is consistent with the lowered value of $10Dq$ for this complex. The steric interactions between the macrocyclic ligands in $[Ni(Bz[9]aneN_3)_2]^{2+}$ can be quantified in terms of close contacts between the benzyl methylene H atoms of one ring [H(10A) and H(10B)] which are found at distances of 2.229 and 2.181 Å from H(25A) and H(23) of the other macrocycle respectively. Modelling of the centrosymmetric *anti* isomer of $[Ni(Bz[9]aneN_3)_2]^{2+}$ was carried out by transposing the coordinates for a $[Ni(Bz[9]aneN_3)]^{2+}$ fragment obtained from the crystal structure determination of the *syn* isomer, and generating a second $Bz[9]aneN_3$ ligand co-ordinated to Ni to give the centrosymmetric *anti*-$[Ni(Bz[9]aneN_3)_2]^{2+}$. Using the XP program of SHELXTL-PC it was therefore possible to work out hypothetical closest contacts within the resultant molecule. It shows closest contacts between H(10B)···H(6′A) and H(10A)···H(6′A) of 1.702 and 2.065 Å respectively, H(6′A) being a methylene proton of the generated macrocycle and H(10A) and H(10B) benzyl protons of the original ligand. Thus, it appears that this generated *anti* isomer is more sterically hindered than the observed *syn* species. The single-crystal structure of $[Ni(Bz[9]aneN_3)_2][BF_4]_2$ was also determined and found to be the same *syn* isomer. Extended reflux of these salts in solution (water) still afforded the *syn* isomer. At present it is not clear whether steric effects alone explain the observed configuration of $[Ni(Bz[9]aneN_3)_2]^{2+}$, although it seems reasonable to assume that electronic effects are also important.

Cyclic voltammetry was performed upon $[Ni(Bz[9]aneN_3)_2][PF_6]_2$ between −2.4 and +1.1 V *vs.* ferrocene–ferrocenium in MeCN over a temperature range of 235 to 298 K. A reversible Ni^{II}–Ni^{III} oxidation was observed at $E_{\frac{1}{2}} = +0.76$ V at a scan rate of 0.1 V s^{-1} at 235 K, with $\Delta E_p = 58$ mV and $I_{pa}/I_{pc} = 1.01$ (Fig. 3). However, upon warming to 298 K

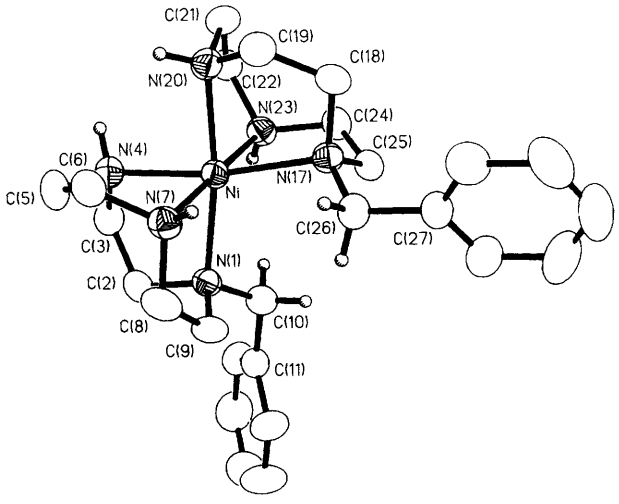

Fig. 2 Structure of $[Ni(Bz[9]aneN_3)_2]^{2+}$ with the numbering scheme adopted

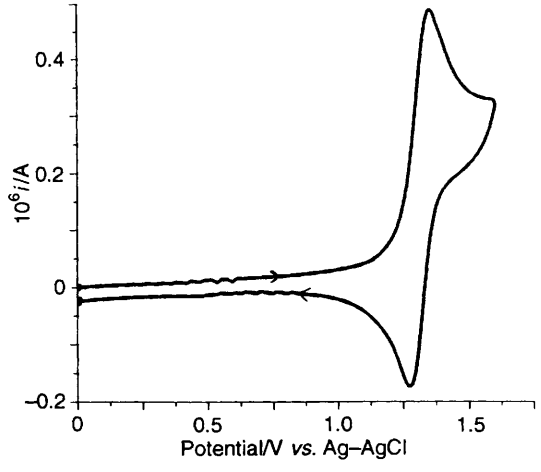

Fig. 3 Cyclic voltammogram of $[Ni(Bz[9]aneN_3)_2][PF_6]_2$ in acetonitrile (0.1 mol dm^{-3} $NBu^n_4BF_4$) at platinum electrodes at 253 K at a scan rate of 0.1 V s^{-1}

this process becomes progressively less reversible (I_{pa}/I_{pc} = 9.09 at 298 K and scan rate of 0.1 V s^{-1}). The electrochemical behaviour of $[Ni([9]aneN_3)_2]Cl_2$ has been reported previously[18–21] and shows a reversible one-electron oxidation at $E_{\frac{1}{2}} = 0.95$ V *vs.* NHE (normal hydrogen electrode) in aqueous solution (0.1 mol dm^{-3} KCl). The complex $[Ni([9]aneN_3)_2][PF_6]_2$ was prepared in order to check the electrochemical measurements in MeCN at platinum electrodes; the Ni^{II}–Ni^{III} couple was observed at $E_{\frac{1}{2}} = +0.55$ V *vs.* ferrocene–ferrocenium at a scan rate of 0.1 V s^{-1} at 298 K, $\Delta E_p = 58$ mV. Thus, under the same conditions, the $[Ni(Bz[9]aneN_3)]^{2+/3+}$ couple is shifted anodically by 0.21 V in comparison to the $[Ni([9]aneN_3)_2]^{2+/3+}$ couple. The crystal structures of both $[Ni([9]aneN_3)_2]^{2+}$[17] and $[Ni([9]aneN_3)_2]^{3+}$[19] have been reported previously, with the average Ni–N distance being observed to shorten from 2.10 to 2.02 Å upon oxidation of Ni^{II} to Ni^{III}. Thus, the presence of the benzylated amine centres appears to destabilise the Ni^{III} because of steric factors, preventing the $Bz[9]aneN_3$ ligand from meeting the requirements of the smaller nickel(III) ion.

Controlled-potential bulk electrolysis of $[Ni(Bz[9]aneN_3)_2][PF_6]_2$ in MeCN at +0.90 V *vs.* ferrocene–ferrocenium at 253 K affords a bright yellow solution, the ESR spectrum of which, measured as a frozen glass at 77 K, exhibits a weak axial signal, with $g_{\|} = 2.03$ and $g_{\perp} = 2.15$. This is consistent with a tetragonally elongated $Ni^{III}N_6$ donor array, and is similar to the reported EPR spectrum[19] of $[Ni([9]aneN_3)_2]^{3+}$ which shows $g_{\|} = 2.03$ and $g_{\perp} = 2.12$.

The ion $[Ni(Bz[9]aneN_3)_2]^{3+}$ is unstable even under an inert atmosphere of Ar or N_2, which contrasts with the stability of the $[Ni([9]aneN_3)_2]^{3+}$ cation. The oxidation was monitored spectroelectrochemically, and the growth of three intense charge-transfer bands observed at ν_{max} 25 250, 33 200 and 40 650 cm^{-1} (Fig. 4). These bands reached a maximum intensity after *ca.* 10–15 min, then started to diminish although current was still being passed through the solution. After 2 h only one weaker band at 41 000 cm^{-1} was observed. Cyclic voltammetry on the oxidised solution did not show a $[Ni(Bz[9]aneN_3)_2]^{2+/3+}$ couple, but, interestingly, showed a reversible couple at $E_{\frac{1}{2}} = +0.55$ V *vs.* ferrocene–ferrocenium in MeCN at 298 K corresponding to the $[Ni([9]aneN_3)_2]^{2+/3+}$ couple. We propose, therefore, that the reactive $[Ni(Bz[9]aneN_3)_2]^{3+}$ species undergoes a decomposition process which appears to proceed *via* loss of the benzyl groups from the macrocyclic ligands to generate $[Ni([9]aneN_3)_2]^{3+}$ as one of the decomposition products.

Palladium

The co-ordination chemistry of $[9]aneN_3$ with Pd^{II} and Pd^{III} has been established independently by both the Edinburgh group[26] and McAuley and co-workers,[27,28] with the single-crystal structures of both $[Pd([9]aneN_3)_2]^{2+}$ and $[Pd([9]aneN_3)_2]^{3+}$ having been reported. The facile oxidation ($E_{\frac{1}{2}} = 0.070$ V *vs.* ferrocene–ferrocenium) from square-planar $[Pd([9]aneN_3)_2]^{2+}$ to tetragonally distorted octahedral $[Pd([9]aneN_3)_2]^{3+}$ has been attributed to fluxionality of the macrocyclic ligands and their ability rapidly to alter their mode of co-ordination.[26–28]

Reaction of $Pd(O_2CMe)_2$ with 2 equivalents of $Bz[9]aneN_3$ followed by addition of NH_4PF_6 affords a yellow solid. Formulation of this material as $[Pd(Bz[9]aneN_3)_2][PF_6]_2$ was confirmed by FAB mass spectrometry and elemental analysis. The electronic spectrum of $[Pd(Bz[9]aneN_3)_2]^{2+}$ exhibits one maximum at ν_{max} 33 550 cm^{-1} ($\varepsilon = 530$ dm^3 mol^{-1} cm^{-1}), which is consistent with a square-planar co-ordination geometry at the Pd^{II}. The ^{13}C NMR spectrum of $[Pd(Bz[9]aneN_3)_2]^{2+}$ exhibits three signals for the macrocyclic ring carbon atoms, implying that the $Bz[9]aneN_3$ ligand maintains its mirror symmetry upon complexation. In order to confirm the structure of the complex a single-crystal determination was undertaken.

Pale yellow blocks of $[Pd(Bz[9]aneN_3)_2][PF_6]_2 \cdot 2MeCN$ of X-ray quality were obtained by the diffusion of Et_2O into an MeCN solution of the complex at 253 K. Details of the structure solution and refinement are given in the Experimental section. Selected bond lengths and angles are given in Table 3, fractional atomic coordinates in Table 4 and a view of the cation in Fig. 5. The Pd^{II} lies on an inversion centre and the ligands are bound *via* two amine donors N(4) and N(7) at distances of 2.0588(19) and 2.0605(19) Å respectively. The macrocycle adopts a [234] conformation according to Dale's notation,[29] with the non-interacting benzyl amine N-donor [N(1)] at a distance of 3.402(4) Å from the metal centre. The structure also contains two MeCN solvate molecules per cation. The aromatic rings are not involved in any inter- or intramolecular π-stacking interactions. The co-ordination sphere of $[Pd(Bz[9]aneN_3)_2]^{2+}$ in the solid state is thus very similar to that reported previously for $[Pd([9]aneN_3)_2][PF_6]_2$. In both structures the non-interacting N-donors of the macrocycles are more than 3.4 Å, and pointing away, from the metal centre.

Cyclic voltammetry was performed upon $[Pd(Bz[9]aneN_3)_2][PF_6]_2$ in MeCN–0.1 mol dm^{-3} $NBu^n_4BF_4$ at 298 K, over the range −2.4 to +1.1 V *vs.* ferrocene–ferrocenium. This is illustrated in Fig. 6(*a*). A fully reversible oxidation is observed at $E_{\frac{1}{2}} = +0.360$ V at a scan rate of 0.10 V s^{-1}, $\Delta E_p = 0.088$ V. At 260 K the peak height of the anodic wave diminished slightly, although not that of the cathodic wave, suggesting that this oxidation involves a significant

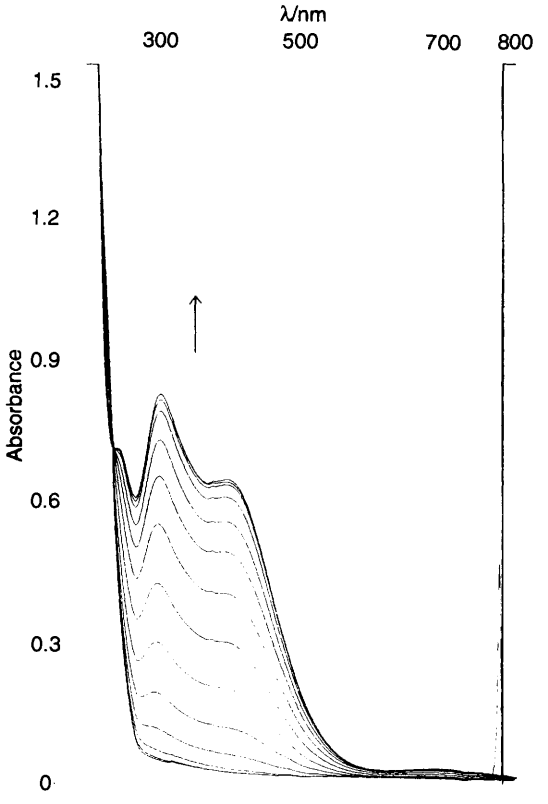

Fig. 4 Electronic absorption spectrum showing the oxidation of $[Ni(Bz[9]aneN_3)_2]^{2+}$ to $[Ni(Bz[9]aneN_3)_2]^{3+}$

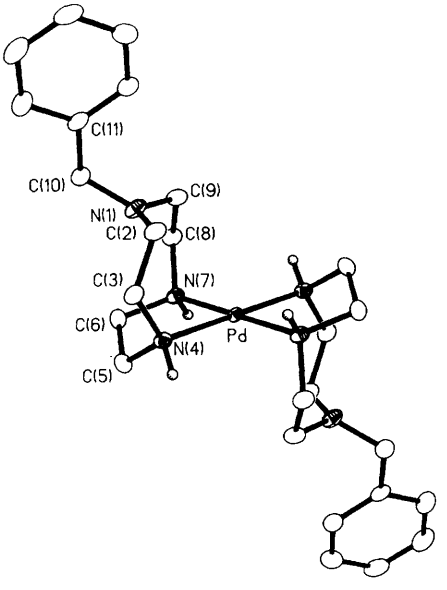

Fig. 5 Structure of $[Pd(Bz[9]aneN_3)_2]^{2+}$ with the numbering scheme adopted

structural rearrangement. Coulometric measurements confirm that the oxidation is a one-electron process affording a deep red solution. This oxidation is accompanied by the appearance of a charge-transfer band in the electronic spectrum at ν_{max} 21 170 cm^{-1} ($\varepsilon = 12\,400$ dm^3 mol^{-1} cm^{-1}). The cyclic voltammogram of the oxidised solution is identical to that of the palladium(II) precursor confirming the reversibility of the oxidation process. A second irreversible oxidation (to Pd^{IV}) is observed at $E_{p_a} = +0.99$ V at a scan rate of 0.10 V s^{-1} [Fig. 6(*b*)]. However this oxidation remains irreversible even at faster scan rates (1.0 V s^{-1}) and lower temperatures (238 K). An irreversible reduction (to Pd^{I}) is observed at −1.61 V; this process

Table 3 Bond lengths (Å), angles and torsion angles (°) for $[Pd(Bz[9]aneN_3)_2]^{2+}$

Pd–N(4)	2.0588(19)	N(4)–C(5)	1.501(3)
Pd–N(7)	2.0605(19)	C(5)–C(6)	1.513(3)
N(1)–C(2)	1.450(3)	C(6)–N(7)	1.511(3)
N(1)–C(9)	1.449(3)	N(7)–C(8)	1.498(3)
N(1)–C(10)	1.458(3)	C(8)–C(9)	1.521(3)
C(2)–C(3)	1.526(3)	C(10)–C(11)	1.524(3)
C(3)–N(4)	1.505(3)		
N(4)–Pd–N(7)	83.49(7)	C(5)–C(6)–N(7)	109.81(18)
C(2)–N(1)–C(9)	120.37(19)	Pd–N(7)–C(6)	110.10(13)
C(2)–N(1)–C(10)	116.22(19)	Pd–N(7)–C(8)	114.08(14)
C(9)–N(1)–C(10)	118.42(19)	C(6)–N(7)–C(8)	111.84(17)
N(1)–C(2)–C(3)	115.02(19)	N(7)–C(8)–C(9)	112.45(19)
C(2)–C(3)–N(4)	115.02(18)	N(1)–C(9)–C(8)	113.58(19)
Pd–N(4)–C(3)	116.87(14)	N(1)–C(10)–C(11)	114.78(19)
Pd–N(4)–C(5)	103.59(13)	C(10)–C(11)–C(12)	118.75(21)
C(3)–N(4)–C(5)	114.37(17)	C(10)–C(11)–C(16)	122.83(21)
N(4)–C(5)–C(6)	108.64(18)		
C(9)–N(1)–C(2)–C(3)	−113.72(23)	N(4)–C(5)–C(6)–N(7)	46.30(23)
C(10)–N(1)–C(2)–C(3)	91.66(24)	C(5)–C(6)–N(7)–C(8)	−144.20(19)
C(2)–N(1)–C(9)–C(8)	110.45(23)	C(6)–N(7)–C(8)–C(9)	85.78(22)
C(10)–N(1)–C(9)–C(8)	−95.48(24)	N(7)–C(8)–C(9)–N(1)	−53.0(3)
C(2)–N(1)–C(10)–C(11)	58.4(3)	N(1)–C(10)–C(11)–C(12)	−147.13(22)
C(9)–N(1)–C(10)–C(11)	−96.70(24)	N(1)–C(10)–C(11)–C(16)	33.0(3)
N(1)–C(2)–C(3)–N(4)	70.1(3)	C(10)–C(11)–C(12)–C(13)	180.00(22)
C(2)–C(3)–N(4)–C(5)	−107.05(22)	C(10)–C(11)–C(16)–C(15)	−178.94(23)
C(3)–N(4)–C(5)–C(6)	75.69(22)		

Table 4 Fractional coordinates for $[Pd(Bz[9]aneN_3)_2]^{2+}$

Atom	*x*	*y*	*z*
Pd	0.0	0.0	0.0
N(1)	0.325 87(22)	0.101 52(20)	0.249 09(17)
C(2)	0.246 1(3)	0.206 80(23)	0.238 31(20)
C(3)	0.257 2(3)	0.294 55(23)	0.131 27(19)
N(4)	0.164 81(21)	0.206 02(19)	0.006 32(16)
C(5)	0.264 45(25)	0.175 40(23)	−0.066 78(20)
C(6)	0.320 62(25)	0.054 91(23)	−0.016 47(20)
N(7)	0.184 17(21)	−0.070 04(19)	0.002 27(16)
C(8)	0.235 3(3)	−0.138 02(23)	0.113 54(20)
C(9)	0.236 0(3)	−0.056 10(23)	0.230 19(20)
C(10)	0.489 5(3)	0.155 94(25)	0.326 97(20)
C(11)	0.513 56(25)	0.214 23(24)	0.459 40(20)
C(12)	0.652 9(3)	0.331 21(25)	0.521 99(22)
C(13)	0.679 7(3)	0.387 50(25)	0.641 97(22)
C(14)	0.567 7(3)	0.329 3(3)	0.701 77(21)
C(15)	0.428 6(3)	0.213 7(3)	0.640 56(21)
C(16)	0.403 5(3)	0.156 02(25)	0.520 48(21)
P	0.181 96(8)	0.557 95(7)	0.837 79(6)
F(1)	0.063 41(17)	0.388 16(15)	0.810 08(13)
F(2)	0.299 50(17)	0.727 07(15)	0.868 10(14)
F(3)	0.049 09(17)	0.608 72(17)	0.866 80(15)
F(4)	0.119 36(21)	0.574 09(17)	0.698 31(13)
F(5)	0.243 07(21)	0.540 55(17)	0.977 78(14)
F(6)	0.313 70(19)	0.507 82(18)	0.808 64(19)
C(1a)	0.038 85(18)	0.267 19(18)	0.524 90(16)
C(2a)	−0.036 62(25)	0.151 72(21)	0.419 71(18)
N(3a)	−0.092 7(3)	0.063 5(3)	0.337 9(3)

showed no signs of reversibility at faster scan rates or lower temperatures.

The $[Pd(Bz[9]aneN_3)_2]^{2+/3+}$ couple is 0.29 V more anodic than that of $[Pd([9]aneN_3)_2]^{2+/3+}$. Upon oxidation from Pd^{II} to Pd^{III} one would expect the metal ion to contract and the steric requirements to change from a square-planar to a distorted-octahedral geometry. The more anodic Pd^{II}–Pd^{III} couple for $[Pd(Bz[9]aneN_3)_2]^{2+}$ can therefore be attributed to the greater steric bulk of the benzyl groups, which inhibit the axial N-donors from fully approaching the metal centre upon oxidation.

Any structural differences between the co-ordination geometries of $[Pd([9]aneN_3)_2]^{3+}$ and $[Pd(Bz[9]aneN_3)_2]^{3+}$ should be reflected in the ESR spectra of the two species. The ESR spectrum of $[Pd([9]aneN_3)_2]^{3+}$ exhibits[26–28] an axial signal with $g_{\|} = 2.007$ and $g_{\perp} = 2.123$. No hyperfine coupling to ^{105}Pd is observed, although superhyperfine coupling to two N-donors is observed in the $g_{\|}$ component giving a quintet (ratio 1:2:3:2:1) with $A_{\|} = 27$ G. This is consistent with the tetragonal distortion which is observed in the crystal structure[26] of $[Pd([9]aneN_3)_2]^{3+}$, Pd–N 2.111(9), 2.118(9) and 2.180(9) Å.

The ESR spectrum of $[Pd(Bz[9]aneN_3)_2]^{3+}$ electrogenerated at +0.50 V *vs.* ferrocene–ferrocenium is shown in Fig. 7. It is broad (probably due to unresolved hyperfine and superhyperfine coupling), but exhibits an axial signal with $g_{\|} = 2.007$ and $g_{\perp} = 2.117$. Superhyperfine coupling is observed to two N-donors (1:2:3:2:1 quintet) in the $g_{\|}$ component, with $A_{\|} = 26.9$ G. These data are very similar to those reported for $[Pd([9]aneN_3)_2]^{3+}$, the only real difference being that the superhyperfine coupling to the axial N-donors is better resolved for $[Pd(Bz[9]aneN_3)_2]^{3+}$. Thus, the ESR data are consistent with a tetragonally elongated octahedral co-ordination geometry for $[Pd(Bz[9]aneN_3)_2]^{3+}$. The axial symmetry in the ESR spectrum of $[Pd(Bz[9]aneN_3)_2]^{3+}$ and the observed superhyperfine coupling suggests that the benzyl amines occupy mutually opposite sites at the metal centre, affording an overall *anti* configuration.

Experimental

All solvents were dried and purified using standard procedures.[30] Tetrahydrofuran (HPLC-grade, Fisons) was distilled from sodium–benzophenone. Electrochemical measurements were carried out in HPLC-grade MeCN (Labscan) without further purification. Dimethylformamide used for macrocycle cyclisation reactions was always taken from a fresh bottle. Standard chemicals were used as commercially supplied. The compound $PhCH_2Br$ (BDH) was distilled on a shortway distillation apparatus then stored at −20 °C prior to use. Infrared spectra were recorded as KBr discs or thin films (on CsI plates) on a Perkin-Elmer 1600 Series FT-IR spectrometer, fast atom bombardment (FAB) and electron ionisation (EI) mass spectra on a Kratos MS 50TC spectrometer, with FAB

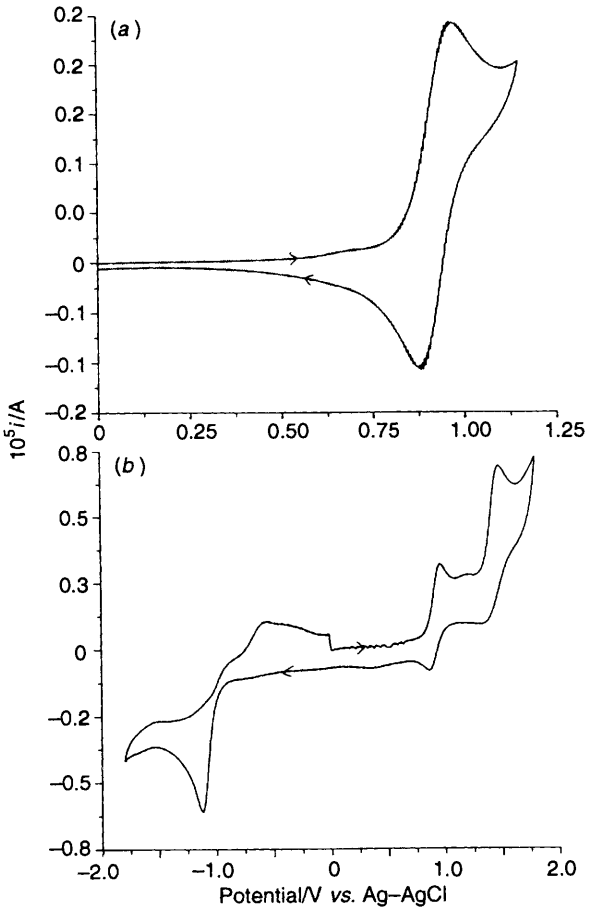

Fig. 6 Cyclic voltammograms of $[Pd(Bz[9]aneN_3)_2][PF_6]_2$ in acetonitrile (0.1 mol dm^{-3} $NBu^n_4BF_4$) at platinum electrodes at 298 K, scan rate 0.1 V s^{-1}

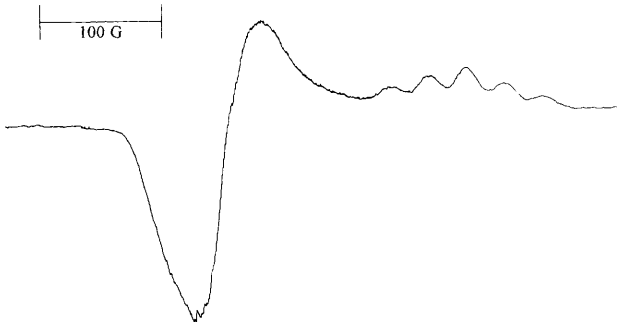

Fig. 7 The ESR spectrum (frozen glass, 77 K, MeCN) of $[Pd(Bz[9]aneN_3)_2]^{3+}$

spectra recorded in a 3-nitrobenzyl alcohol matrix. Elemental analyses were performed by the University of Edinburgh Chemistry Department microanalytical service. Electronic spectra were recorded on a Perkin-Elmer Lambda-9 spectrometer using 1 cm matched quartz cells. An optically transparent electrode (OTE) system designed and built in the University of Edinburgh was employed to perform *in situ* spectroelectrochemistry. A fine Pt/Rh gauze working electrode was used in conjunction with a platinum-wire auxiliary and a Ag–AgCl reference electrode, both separated from the solution by porous glass frits to give a three-compartment system. The cell was mounted in a Perkin-Elmer Lambda-9 spectrometer. Temperature control was maintained by the passage of dry, pre-cooled N_2 gas around the cell and monitored with a thermocouple/digital thermometer.

Cyclic voltammetry was performed using a conventional three-electrode cell with platinum-counter and micro working electrodes and a Ag–AgCl reference electrode. Data were recorded and manipulated using a DSL 286-D personal computer with General Purpose Electrochemical System (GPES) Version 3 software connected to an Autolab system containing a PSTAT10 potentiostat. Controlled-potential electrolysis was carried out using the GPES system employing a three-electrode H-type cell with platinum-basket working electrode. X-Band EPR spectra were recorded on a Brüker ER-2000 spectrometer, employing 100 kHz field modulation, as frozen glasses at 77 K under an atmosphere of N_2. Proton NMR spectra were recorded on Brüker WP80, WP200 and AC250 spectrometers, operating at 80.13, 200.13 and 250.13 MHz respectively, ^{13}C NMR spectra on Brüker WP200 and AC250 spectrometers, operating at 50.32 and 62.89 MHz respectively.

1,4,7-Triazacyclononane was prepared by a standard literature procedure.[31,32] The preparation of 1,4,7-triazatricyclo[5.2.1.$0^{4,10}$]decane from 1,4,7-triazacyclononane was carried out according to the method reported by Atkins.[12]

Preparations

1-Benzyl-4-formyl-1,4,7-triazacyclononane. This compound was prepared according to the method of Weisman *et al.*[14] 1,4,7-Triazatricyclo[5.2.1.$0^{4,10}$]decane (0.50 g, 3.6 mmol) and $PhCH_2Br$ (0.615 g, 3.6 mmol) were stirred in thf (2 cm^3) for 1 h to yield a thick paste. Diethyl ether (10 cm^3) was added and the solution filtered to afford a white solid. This was dissolved in water (10 cm^3) and refluxed for 3.5 h. The solution was adjusted to pH 12 with sodium hydroxide solution (5 mol dm^{-3}) and the product extracted with $CHCl_3$ (5 × 50 cm^3). The combined extracts were dried ($MgSO_4$) and the solvent removed under reduced pressure to give the product as a yellow oil, which was stored as a standard solution in ethanol at −20 °C (0.80 g, 89.9%). NMR ($CDCl_3$): ^1H (200.13 MHz), δ 2.35–3.25 (12 H, m, NCH_2, ring), 3.49 (2 H, s, NCH_2Ph), 7.13 (5 H, br s, aryl H), 7.79 and 7.93 (1 H, s, NCHO, from alternative isomers); ^{13}C (50.32 MHz), δ 45.93, 46.03, 46.37, 47.13, 47.33, 48.19, 49.39, 51.45, 52.12, 54.73, 56.51 (NCH_2, ring, from alternative isomers, assuming one coincidence), 61.54 (NCH_2Ph, assuming both isomers coincident), 126.33, 126.53, 127.59, 127.70, 128.26 (aromatic CH, assuming one coincidence), 138.04 (aromatic quaternary, assuming both isomers coincident), 163.01 and 163.17 (NCHO, from alternative isomers) (Found: C, 67.4; H, 9.10; N, 16.9. $C_{14}H_{21}N_3O$ requires C, 68.0; H, 8.55; N, 17.0%).

1-Benzyl-1,4,7-triazacyclononane (Bz[9]aneN$_3$). 1-Benzyl-4-formyl-1,4,7-triazacyclononane (0.3 g, 1.2 mmol) was added to KOH (1.48 g, 26 mmol) in EtOH (10 cm^3) and this mixture was refluxed for 24 h. The solvent was then removed *in vacuo* and the residue taken up in water (5 cm^3). The solution was extracted with $CHCl_3$ (5 × 25 cm^3), the combined extracts were dried ($MgSO_4$) and the solvent removed under reduced pressure to give a yellow oil. This was distilled on a shortway bulb-to-bulb distillation apparatus to give the product as a clear viscous oil which was stored as a standard solution in ethanol at −20 °C (0.251 g, 95.1%). NMR ($CDCl_3$): ^1H (200.13 MHz), δ 2.46–2.59 (12 H, m, NCH_2 ring), 3.53 (2 H, s, NCH_2Ph) and 7.14 (5 H, m, aryl H); ^{13}C (50.32 MHz), δ 45.77, 45.96, 52.08 (NCH_2, ring), 60.97 (NCH_2Ph), 126.37, 127.65, 128.32 (aromatic CH) and 139.08 (aromatic quaternary). EI mass spectrum: *m/z* 219 ($Bz[9]aneN_3^+$).

[Ni(Bz[9]aneN$_3$)$_2$][PF$_6$]$_2$. The compound Bz[9]aneN$_3$ (0.075 g, 0.34 mmol) and $[Ni(H_2O)_6][NO_3]_2$ (0.05 g, 0.17 mmol) were dissolved in ethanol (15 cm^3). After standing for 2 h the solution had changed to purple-blue and a fine pink precipitate had formed, which was collected and dissolved in water (10 cm^3). The salt NH_4PF_6 (0.055 g, 0.34 mmol) was added as a solution in water (5 cm^3) to yield a pink precipitate, then acetone until the solution cleared and upon evaporation

pink needles were obtained (0.030 g, 22.3%) (Found: C, 38.8; H, 5.70; N, 10.7. $C_{26}H_{42}F_{12}N_6NiP_2$ requires C, 39.7; H, 5.40; N, 10.7%). IR (KBr disc): 3278m, 2971w, 1490m, 1424m, 856s and 558 cm^{-1}. FAB mass spectrum: m/z = 515, $[Ni(Bz[9]aneN_3)_2(PF_6)]^+$ and 496, $[Ni(Bz[9]aneN_3)_2]^+$. Electronic spectrum: ν_{max} (ε_{max}) 10 408 (11), 11 904 (sh), 18 798 (6) and 25 641 cm^{-1} (18 dm^3 mol^{-1} cm^{-1}).

$[Pd(Bz[9]aneN_3)_2][PF_6]_2$. The compound $Pd(O_2CMe)_2$ (0.051 g, 0.23 mmol) and $Bz[9]aneN_3$ (0.10 g, 0.46 mmol) were dissolved in CH_2Cl_2 (15 cm^3) and the solution was stirred at room temperature for 2 h. This resulted in a change from orange to pale yellow. The solvent was removed *in vacuo* and the residue taken up in the minimum volume of methanol. This solution was filtered and NH_4PF_6 (0.081 g, 0.50 mmol) was added as a solution in water (5 cm^3). A yellow microcrystalline solid was obtained upon standing at 5 °C for 24 h. This was collected and recrystallised by diffusion of diethyl ether into an acetonitrile solution (0.082 g, 43.3%). NMR (CD_3NO_2): ^1H (80.13 MHz), δ 2.5–4.0 (12 H, m, CH_2 ring), 4.22 (2 H, s, CH_2Ph) and 7.41 (5 H, m, aryl H); ^{13}C (50.32 MHz), δ 52.46, 52.54, 54.82 (CH_2 ring), 57.98 (CH_2Ph), 126.63, 127.73, 128.47 (aromatic CH) and 136.03 (aromatic quaternary) (Found: C, 37.1; H, 5.30; N, 9.85. $C_{26}H_{42}F_{12}N_6P_2Pd$ requires C, 37.4; H, 5.05; N, 10.1%). IR (KBr disc): 2930w, 2451m, 1452m, 1362w, 1076m, 836s and 558s cm^{-1}. FAB mass spectrum: m/z = 689, $[Pd(Bz[9]aneN_3)_2(PF_6)]^+$; 543, $[Pd(Bz[9]aneN_3)_2]^+$ and 324, $[Pd(Bz[9]aneN_3)]^+$.

Single-crystal structure determinations

$[Ni(Bz[9]aneN_3)_2][PF_6]_2$. Crystals suitable for X-ray analysis were obtained by the slow evaporation of a solution of the complex in a thf–acetone–water mixture.

Crystal data. $C_{26}H_{42}F_{12}N_6NiP_2$, M = 787.31, monoclinic, space group $P2_1/n$, a = 14.8184(19), b = 13.3581(16), c = 18.267(2) Å, β = 112.016(8)°, U = 3352 $Å^3$ [from 2θ values of 47 reflections measured at ±ω (22 ≤ 2θ ≤ 24°), λ = 0.710 73 Å, T = 295 K], Z = 4, D_c = 1.560 g cm^{-3}. Crystal dimensions 1.05 × 0.19 × 0.08 mm, μ(Mo-Kα) = 0.770 mm^{-1}, $F(000)$ = 1624.

Data collection and processing. Stoë STADI-4 four-circle diffractometer equipped with an Oxford Cryosystems low-temperature device,[33] ω–2θ scan mode using the learnt-profile method.[34] Graphite-monochromated Mo-Kα radiation: 4383 unique data collected ($2\theta_{max}$ = 45°, $-15 \leqslant h \leqslant 14$, $0 \leqslant k \leqslant 14$, $0 \leqslant l \leqslant 19$), of which 4346 were used in all calculations; 5% crystal decay. An absorption correction was applied using ψ scans (maximum and minimum transmission factors 0.785 and 0.747 respectively).

Structure analysis and refinement. The structure was solved using direct methods SHELXS 86,[35] then refined on F^2 using SHELXL 93.[36] All non-H atoms were refined with anisotropic thermal parameters and H atoms were fixed in calculated positions. At final convergence $R[F \geqslant 4\sigma(F)]$ = 0.0431, $wR(F^2$, all data) = 0.1285, $S(F^2)$ = 1.12 for 425 parameters. The weighting scheme $w^{-1} = [\sigma^2(F_o^2) + (0.0433P)^2 + 5.1174P]$, $P = \frac{1}{3}[\max(F_o^2, 0) + 2F_c^2]$ gave satisfactory agreement analyses. The final Fourier-difference synthesis contained no peak above +0.53 and no trough below −0.33 e $Å^{-3}$.

$[Pd(Bz[9]aneN_3)_2][PF_6]_2 \cdot 2MeCN$. Crystals suitable for X-ray studies were obtained from the diffusion of ether vapour into an acetonitrile solution of the complex at −20 °C.

Crystal data. $C_{30}H_{48}F_{12}N_8P_2Pd$, M = 916.97, triclinic, space group $P\bar{1}$, a = 9.421(6), b = 9.695(6), c = 11.437(7) Å, α = 92.43(5), β = 105.45(5), γ = 109.74(5)°, U = 937.5 $Å^{-3}$ [from 2θ values of 13 reflections measured at ±ω(30 ≤ 2θ ≤ 32°), λ = 0.710 73 Å, T = 150 K], Z = 1, D_c = 1.624 g cm^{-3}. Crystal dimensions 0.74 × 0.39 × 0.31 mm, μ(Mo-Kα) = 0.664 mm^{-1}, $F(000)$ = 468.

Data collection and processing. Details as above except 2552 data collected ($-10 \leqslant h \leqslant 9$, $-10 \leqslant k \leqslant 10$, $0 \leqslant l \leqslant 12$), 2376 unique data ($R_{int}$ = 0.0123) giving 2347 with $F > 4\sigma(F)$. No crystal decay. An absorption correction was applied using ψ scans (maximum and minimum transmission factors 0.822 and 0.767 respectively).

Structure analysis and refinement. The position of the palladium atom was fixed at (0,0,0) as a trial position and successive cycles of least-squares and Fourier-difference synthesis using SHELX 76[37] and confirmed the position of the palladium atom and located all non-H atoms. All non-H atoms were refined anisotropically and H atoms were fixed in calculated positions. During refinement, the CH_3 group of the MeCN solvate molecule was found to be disordered by rotation around the C–C–N axis. This was modelled using two distinct, equally occupied orientations with restrained C–H and H–H distances. At final convergence R = 0.0241, R' = 0.0372, S = 2.698 for 266 parameters. The weighting scheme $w^{-1} = \sigma^2(F) + 0.0001F^2$ gave satisfactory agreement analyses. The final Fourier-difference synthesis contained no peak above +0.63 and no trough below −0.53 e $Å^{-3}$. Molecular plots were generated using SHELXTL-PC.[38]

Complete atomic coordinates, thermal parameters and bond lengths and angles have been deposited at the Cambridge Crystallographic Data Centre. See Instructions for Authors, *J. Chem. Soc., Dalton Trans.*, 1996, Issue 1.

Acknowledgements

We thank the University of Edinburgh for a studentship (to S. A. R.) and Mr. Eric McInnes for assistance with electrochemical, EPR and OTE measurements. We also thank the EPSRC and The Royal Society for support.

References

1 P. Chaudhuri and K. Wieghardt, *Prog. Inorg. Chem.*, 1987, **35**, 329.
2 K. Wieghardt, *Pure Appl. Chem.*, 1988, **60**, 509.
3 P. Chaudhuri, M. Guttmann, D. Ventur, K. Wieghardt, B. Nuber and J. Weiss, *J. Chem. Soc., Chem. Commun.*, 1985, 1618.
4 K. Wieghardt, P. Chaudhuri, B. Nuber and J. Weiss, *Inorg. Chem.*, 1982, **21**, 3086.
5 G. Haselhorst, S. Stoetzel, A. Strassburger, W. Walz, K. Wieghardt and B. Nuber, *J. Chem. Soc., Dalton Trans.*, 1993, 83.
6 T. Beissel, B. S. P. C. Della Vedova, K. Wieghardt and R. Boese, *Inorg. Chem.*, 1990, **29**, 1736.
7 A. Shaver, in *Comprehensive Coordination Chemistry*, eds. G. Wilkinson, R. D. Gillard and J. A. McCleverty, Pergamon, Oxford, 1987, vol. 2, ch. 13.6.
8 N. J. Coville, K. E. Duplooy and W. Pickl, *Coord. Chem. Rev.*, 1992, **116**, 1.
9 N. E. Watts, in *Comprehensive Organometallic Chemistry*, eds. G. Wilkinson, F. G. A. Stone and E. W. Abel, Pergamon, Oxford, 1982, vol. 8, ch. 59.
10 G. R. Weisman, V. Johnson and R. E. Fiala, *Tetrahedron Lett.*, 1980, 3635.
11 J. M. Erhardt and J. D. Wuest, *J. Am. Chem. Soc.*, 1980, **102**, 6363.
12 T. J. Atkins, *J. Am. Chem. Soc.*, 1980, **102**, 6364.
13 A. J. Blake, I. A. Fallis, R. O. Gould, S. G. Harris, S. Parsons, S. A. Ross and M. Schröder, *Acta Crystallogr., Sect. C*, 1995, **51**, 738.
14 G. R. Weisman, D. J. Vachon, V. B. Johnson and D. A. Gronbeck, *J. Chem. Soc., Chem. Commun.*, 1987, 886.
15 A. J. Blake, I. A. Fallis, R. O. Gould, S. Parsons, S. A. Ross and M. Schröder, *J. Chem. Soc., Chem. Commun.*, 1994, 2467.
16 R. Yang and L. J. Zompa, *Inorg. Chem.*, 1976, **15**, 1499.
17 L. J. Zompa and T. N. Margulis, *Inorg. Chim. Acta*, 1978, **28**, 1157.
18 K. Wieghardt, W. Schmidt, W. Herrmann and H.-J. Küppers, *Inorg. Chem.*, 1983, **22**, 2953.
19 K. Wieghardt, W. Walz, B. Nuber, J. Weiss, A. Ozarowski, H. Stratemeier and D. Reinen, *Inorg. Chem.*, 1986, **25**, 1650.
20 A. McAuley, P. R. Norman and O. Olubuyide, *Inorg. Chem.*, 1984, **23**, 1938.
21 A. McAuley, P. R. Norman and O. Olubuyide, *J. Chem. Soc., Dalton Trans.*, 1984, 1501.
22 R. D. Hancock, *Prog. Inorg. Chem.*, 1989, **37**, 187.

23 A. B. P. Lever, *Inorganic Electronic Spectroscopy*, Elsevier, Amsterdam, 1968.
24 M. A. Robinson, J. D. Curry and D. H. Busch, *Inorg. Chem.*, 1963, **2**, 1178.
25 G. Reid and M. Schröder, *Chem. Soc. Rev.*, 1990, **19**, 239.
26 A. J. Blake, L. M. Gordon, A. J. Holder, T. I. Hyde, G. Reid and M. Schröder, *J. Chem. Soc., Chem. Commun.*, 1988, 1452.
27 G. Hunter, A. McAuley and T. W. Whitcombe, *Inorg. Chem.*, 1988, **27**, 2634.
28 A. McAuley and T. W. Whitcombe, *Inorg. Chem.*, 1988, **27**, 3090.
29 J. Dale, *Acta Chem. Scand.*, 1973, **27**, 1115.
30 D. D. Perrin, D. R. Perrin and W. L. F. Armarego, *Purification of Laboratory Chemicals*, 2nd edn., Pergamon, Oxford, 1980.
31 H. Koyama and T. Yoshino, *Bull. Chem. Soc. Jpn.*, 1972, **45**, 481.
32 J. E. Richman and T. J. Atkins, *J. Am. Chem. Soc.*, 1974, **96**, 2268.
33 J. Cosier and A. M. Glazer, *J. Appl. Crystallogr.*, 1986, **19**, 105.
34 W. Clegg, *Acta Crystallogr., Sect. C*, 1990, **47**, 22.
35 G. M. Sheldrick, SHELXS 86, program for crystal structure solution; *Acta Crystallogr., Sect. A*, 1990, **46**, 467.
36 G. M. Sheldrick, SHELXL 93, program for crystal structure refinement, University of Göttingen, 1993.
37 G. M. Sheldrick, SHELX 76, program for crystal structure determination, University of Cambridge, 1976.
38 G. M. Sheldrick, SHELXTL-PC, version 4.3, Siemens Analytical X-Ray Instruments Inc., Madison, WI, 1992.

Received 15*th June* 1995; *Paper* 5/03874J